Article
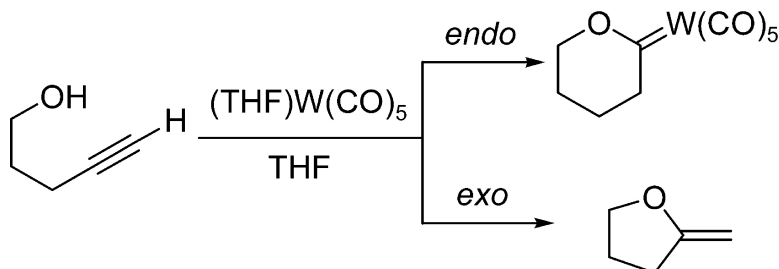
Solvent-Assisted New Reaction Pathways for the (THF)W(CO)-Promoted *endo*- and *exo*-Cycloisomerization of 4-Pentyn-1-ol: A Theoretical Investigation

Toms Sordo, Pablo Campomanes, Alejandro Diguez, Flix Rodrguez, and Francisco J. Faans

More About This Article

Additional resources and features associated with this article are available within the HTML version:

- Supporting Information
- Links to the 11 articles that cite this article, as of the time of this article download
- Access to high resolution figures
- Links to articles and content related to this article
- Copyright permission to reproduce figures and/or text from this article

View the Full Text HTML

Solvent-Assisted New Reaction Pathways for the (THF)W(CO)₅-Promoted *endo*- and *exo*-Cycloisomerization of 4-Pentyn-1-ol: A Theoretical Investigation

Tomás Sordo,* Pablo Campomanes, Alejandro Diéguez, Félix Rodríguez, and
Francisco J. Fañanás

*Contribution from the Departamento de Química Física y Analítica and
Instituto Universitario de Química Organometálica "Enrique Moles",
Universidad de Oviedo, Julián Clavería, 8; E-33006 Oviedo, Spain*

Received July 23, 2004; E-mail: tsordo@uniovi.es

Abstract: New solvent-assisted mechanistic routes were located for the (THF)W(CO)₅-promoted *endo*- and *exo*-cycloisomerization of 4-pentyn-1-ol using the B3LYP/6-31G* (with the LANL2DZ relativistic pseudopotential for W) theory level. A mixed model was used by explicitly including a THF molecule as a component of the reactive system and taking into account the effect of bulk solvent by means of the PCM-UAHF method. This THF molecule plays a crucial role by making the *endo* route leading to the cyclic carbene complex the most favorable one because of an important catalytic effect. These new mechanisms allow a satisfactory rationalization of experimental facts.

Introduction

The design and development of truly efficient, clean, and fast methods to get architectural complex molecules from simple starting materials is probably the most important challenge in modern synthetic and pharmaceutical chemistry.[1] In particular, much work has been devoted to the design of effective routes to cyclic compounds. In this field, organotransition-metal compounds offer many attractive possibilities to build rings not easily available through conventional methods.[2] The alkynol cycloisomerization[3,4] promoted by group 6 metallic complexes is one of these interesting transformations widely utilized in recent years for the synthesis of biologically interesting compounds.[5]

As part of a new project directed to the synthesis of some six-membered cyclic Fischer carbene complexes of type **1** and dihydropyrans **2**, we became interested in the (THF)W(CO)₅-promoted *endo*-cycloisomerization reaction of substituted 4-alkyn-1-ol derivatives (Scheme 1).

A mechanism for these cycloisomerizations that explains the formation of *endo*- and *exo*-cyclization products is depicted in Scheme 2.[3,6] In an initial step, the alkyne is coordinated to the metal fragment to give the corresponding η^2-alkyne complex

Scheme 1
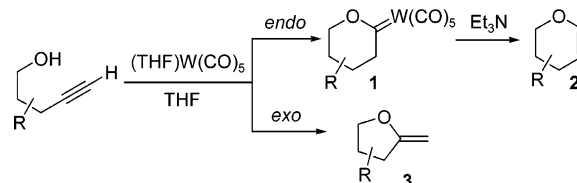
Scheme 2
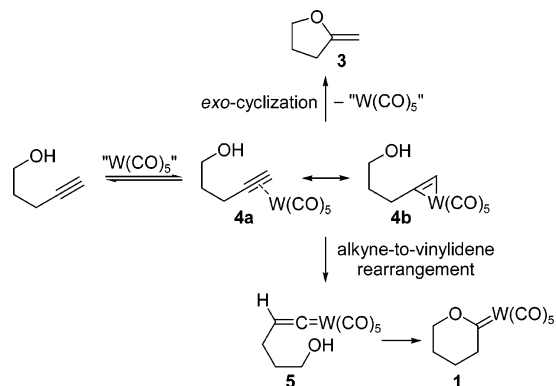
4a, which can be also represented as the metallocyclopropene **4b**. Formation of the *exo*-product **3** can be explained by addition of the hydroxyl group to the internal position of the alkyne followed by elimination of the metal fragment. Alternatively, **4** can rearrange to the vinylidene complex **5** via direct hydride transfer[7] or oxidative addition followed by a formal 1,3-hydride shift.[8] Intramolecular nucleophilic attack of the hydroxyl func-

(1) (a) *The New Chemistry*; Hall, N., Ed.; Cambridge University Press: Cambridge, U.K., 2001. (b) *Stimulating Concepts in Chemistry*; Vögtle, F., Stoddart, J. F., Shibasaki, M., Eds.; Wiley-VCH: Weinheim, Germany, 2000.
(2) (a) Frühauf, H.-W. *Chem. Rev.* **1997**, *97*, 523. (b) Lautens, M.; Klute, W.; Tam, W. *Chem. Rev.* **1996**, *96*, 49.
(3) Weyershausen, B.; Dötz, K. H. *Eur. J. Inorg. Chem.* **1999**, 1057.
(4) McDonald, F. E. *Chem.−Eur. J.* **1999**, *5*, 3103.
(5) For some leading examples, see: (a) Parker, K. A.; Chang, W. *Org. Lett.* **2003**, *5*, 3891. (b) McDonald, F. E.; Reddy, K. S. *Angew. Chem., Int. Ed.* **2001**, *40*, 3653. (c) Bowman, J. L.; McDonald, F. E. *J. Org. Chem.* **1998**, *63*, 3680. (d) Dötz, K. H.; Ehlenz, R. *Chem.−Eur. J.* **1997**, *3*, 1751. (e) McDonald, F. E.; Gleason, M. M. *J. Am. Chem. Soc.* **1996**, *118*, 6648.
(6) Wipf, P.; Graham, T. H. *J. Org. Chem.* **2003**, *68*, 8798.

(7) Silvestre, J.; Hoffmann, R. *Helv. Chim. Acta* **1985**, *68*, 1461.
(8) Wolf, J.; Werner, H.; Serhadli, O.; Ziegler, M. L. *Angew. Chem., Int. Ed. Engl.* **1983**, *22*, 414.

Scheme 3
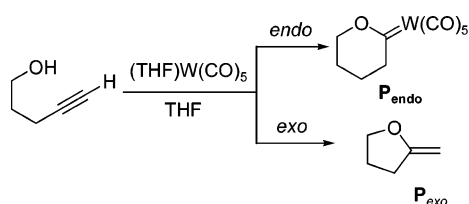
tion at the α-carbon atom of the vinylidene complex leads to the formal *endo*-cyclization complex **1**.

In most of the cases this process has proven to be highly regioselective, providing only the *endo* product **1**.[4] A theoretical study, which supports these observations, has found the *endo* route more favorable than the *exo* one by 20.1 kcal mol⁻¹.[9] However, in our preliminary experiments in this field, we have found that in several cases the reaction is not selective, and mixtures of the formal *endo-* and *exo-*cyclization products (**1**/**2** and **3**) are obtained. A careful revision of the bibliography shows that *endo*/*exo* mixtures have also been observed by other authors with related systems.[4,6,10] These results seem to indicate that the difference between the rate-determining energy barriers for these *endo-* and *exo-*cycloisomerization pathways should be not as large as theoretically found.[9] Moreover, it is known that in the absence of an amine the W(CO)₅-promoted cycloisomerization reaction of 4-alkynols leads to the cyclic carbene complexes **1**, but not to enol ethers **2**.[11] Nevertheless, in the above-mentioned theoretical study the most favorable route leads surprisingly to the enol ether analogous to **2** despite not having taken into account the presence of an amine.

All these facts made us undertake a theoretical study of the (THF)W(CO)₅-promoted cycloisomerization reaction of 4-pentyn-1-ol directed to the search of new reaction pathways leading to the six-membered cyclic Fischer carbene complex **P**_*endo*_ and the five-membered cyclic structure **P**_*exo*_, which better rationalized experimental facts (Scheme 3).

Computational Details

Full geometry optimizations were performed with the B3LYP density functional method (DFT),[12] using the relativistic effective core pseudo-potential LANL2DZ[13] for tungsten and the 6-31G* basis set for the remaining atoms. All calculations were carried out with the Gaussian 98 series of programs.[14] The nature of the stationary points located was further checked, and zero-point vibrational energies (ZPVE) were evaluated by analytical computations of harmonic vibrational frequencies at the same theory level. Intrinsic reaction coordinate calculations

were also carried out to check the connection between the transition states (TS) and the minimum energy structures using the Gonzalez and Schlegel method[15] implemented in Gaussian 98.

ΔG_gas values were also calculated within the ideal gas, rigid rotor, and harmonic oscillator approximations.[16] A pressure of 1 atm and a temperature of 298.15 K were assumed in the calculations.

To take into account condensed-phase effects, we used a self-consistent reaction-field (SCRF) model proposed for quantum chemical computations on solvated molecules.[17] The solvent is represented by a dielectric continuum characterized by its relative static dielectric permittivity ε. The solute, which is placed in a cavity created in the continuum after spending some cavitation energy, polarizes the continuum, which in turn creates an electric field inside the cavity. This interaction can be taken into account using quantum chemical methods by minimizing the electronic energy of the solute plus the Gibbs energy change corresponding to the solvation process.[18] Addition to ΔG_gas of the solvation Gibbs energy gives ΔG_soln. Within the different approaches that can be followed to calculate the electrostatic potential created by the polarized continuum in the cavity, we have employed the polarizable continuum model (PCM)[19] with the united atom Hartree−Fock (UAHF) parametrization.[20] The solvation Gibbs energies ΔG_solvation along the reaction coordinate were evaluated from single-point PCM calculations on the gas-phase-optimized geometries at the same theory level. A relative permittivity of 7.58 was employed to simulate THF as solvent used in the experimental work.

Results and Discussion

The relative electronic energies and Gibbs energies in solution obtained in the present work are collected in Tables 1 and 2. Unless otherwise stated, relative Gibbs energies in solution will be discussed in the text.

We investigated first the *endo-* and *exo-*cycloisomerizations of 4-pentyn-1-ol modeling the effect of solvent as a bulk by the PCM-UAHF method. The initial step for both processes is the barrierless coordination of the W(CO)₅ fragment to the alkyne.[9] Therefore, we initiate our discussion from the alkyne-W(CO)₅ complex **M1** in which the W center presents an octahedral coordination the triple bond of the alkynol being asymmetrically bonded to the metal with W−C distances of 2.427 and 2.554 Å.

We located a new *endo* route leading to the cyclic carbene complex **P**_*endo*_ (Figure 1). Along this new pathway, **M1** evolves through the TS **TS12**_*endo*_ (15.6 kcal mol⁻¹) for H migration from C_α to C_β, while W is bonded to C_α to form the vinylidene complex **M2**_*endo*_ (1.0 kcal mol⁻¹). At **M2**_*endo*_, the W−C_α bond length (2.026 Å) corresponds to a double bond, and the C_α−C_β bond distance (1.310 Å) indicates the cleavage of one of the π-bonds of the original triple bond. **M2**_*endo*_ gives the cyclic structure **M3**_*endo*_ (6.9 kcal mol⁻¹) through the TS **TS23**_*endo*_ (7.4 kcal mol⁻¹) for the intramolecular nucleophilic attack of the

(9) Sheng, Y.; Musaev, D. G.; Reddy, K. S.; McDonald, F. E.; Morokuma, K. *J. Am. Chem. Soc.* **2002**, *124*, 4149.
(10) McDonald, F. E.; Reddy, K. S.; Díaz, Y. *J. Am. Chem. Soc.* **2000**, *122*, 4304.
(11) McDonald, F. E.; Bowman, J. L. *Tetrahedron Lett.* **1996**, *37*, 4675.
(12) (a) Becke, A. B. *J. Chem. Phys.* **1993**, *98*, 5648. (b) Becke, A. B. *Phys. Rev. A* **1988**, *38*, 3098. (c) Lee, C.; Yang, W.; Parr, R. G. *Phys. Rev. B* **1988**, *37*, 785.
(13) Hay, P. J.; Wadt, W. R. *J. Chem. Phys.* **1985**, *82*, 270.
(14) Frisch, M. J.; Trucks, G. W.; Schlegel, H. B.; Scuseria, G. E.; Robb, M. A.; Cheeseman, J. R.; Zakrzewski, V. G.; Montgomery, J. A., Jr.; Stratmann, R. E.; Burant, J. C.; Dapprich, S.; Millam, J. M.; Daniels, A. D.; Kudin, K. N.; Strain, M. C.; Farkas, O.; Tomasi, J.; Barone, V.; Cossi, M.; Cammi, R.; Mennucci, B.; Pomelli, C.; Adamo, C.; Clifford, S.; Ochterski, J.; Petersson, G. A.; Ayala, P. Y.; Cui, Q.; Morokuma, K.; Malick, D. K.; Rabuck, A. D.; Raghavachari, K.; Foresman, J. B.; Cioslowski, J.; Ortiz, J. V.; Stefanov, B. B.; Liu, G.; Liashenko, A.; Piskorz, P.; Komaromi, I.; Gomperts, R.; Martin, R. L.; Fox, D. J.; Keith, T.; Al-Laham, M. A.; Peng, C. Y.; Nanayakkara, A.; Gonzalez, C.; Challacombe, M.; Gill, P. M. W.; Johnson, B. G.; Chen, W.; Wong, M. W.; Andres, J. L.; Head-Gordon, M.; Replogle, E. S.; Pople, J. A. *Gaussian 98*, revision A.6; Gaussian, Inc.: Pittsburgh, PA, 1998.

(15) (a) Gonzalez, C.; Schlegel, H. B. *J. Chem. Phys.* **1989**, *90*, 2154. (b) Gonzalez, C.; Schlegel, H. B. *J. Phys. Chem.* **1990**, *84*, 5523.
(16) McQuarrie, D. A. *Statistical Mechanics*; Harper & Row: New York, 1986.
(17) (a) Rivail, J. L.; Rinaldi, D.; Ruiz-López, M. F. In *Theoretical and Computational Model for Organic Chemistry*; Formosinho, S. J., Csizmadia, I. G., Arnaut, L., Eds.; NATO ASI Series C; Kluwer Academic Publishers: Dordrecht, The Netherlands, 1991; p 339. (b) Cramer, C. J.; Truhlar, D. G. In *Reviews in Computational Chemistry*; Lipkowitz, K. B., Boyd, D. B., Eds.; VCH: New York, 1995; p 6. (c) Rivail, J. L.; Rinaldi, D. In *Computational Chemistry: Review of Current Trends*; Leszczynski, J., Ed.; World Scientific: New York, 1995. (d) Cramer, C. J.; Truhlar, D. G. *Chem. Rev.* **1999**, *99*, 2161.
(18) Claverie, P. In *Quantum Theory of Chemical Reactions*; Daudel, R., Pullman, A., Salem, L., Veillard, A., Eds.; Reidel: Dordrecht, The Netherlands, 1982; p 3.
(19) (a) Tomasi, J.; Persico, M. *Chem. Rev.* **1994**, *94*, 2027. (b) Tomasi, J.; Cammi, R. *J. Comput. Chem.* **1996**, *16*, 1449.
(20) Barone, V.; Cossi, M.; Tomasi, J. *J. Chem. Phys.* **1997**, *107*, 3210.
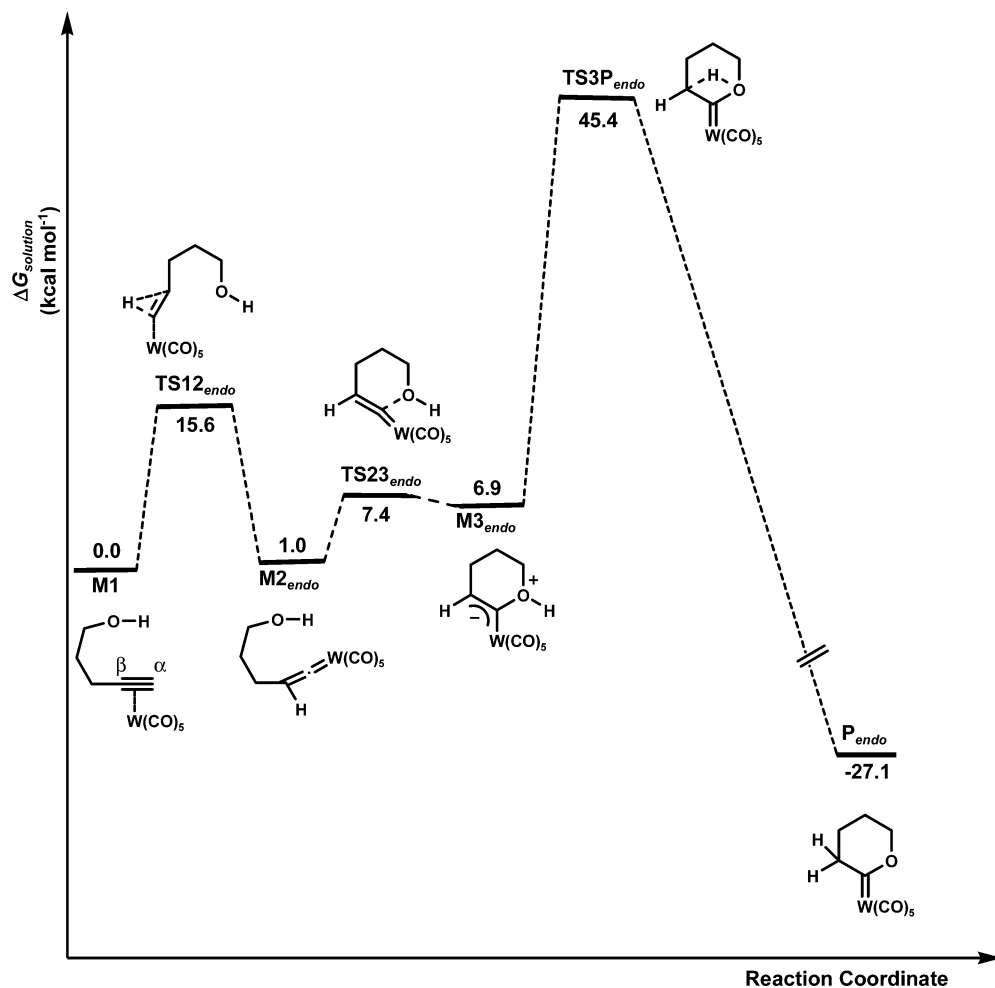
Figure 1. Gibbs energy profile in solution for the *endo*-cycloisomerization of 4-pentyn-1-ol leading to the carbene complex **P**$_{endo}$.

Table 1. Relative Electronic Energies and Relative Gibbs Energies in Solution (in kcal mol^{-1}) Corresponding to All the Critical Structures Located along the Reaction Coordinate for the *endo*- and *exo*-Cycloisomerization of 4-Pentyn-1-ol

structures	ΔE_{elec}	ΔG_{soln}
endo Pathways		
M1	0.0	0.0
TS12$_{endo}$	23.0	15.6
M2$_{endo}$	1.6	1.0
TS23$_{endo}$	8.2	7.4
M3$_{endo}$	8.1	6.9
TS34$_{endo}$	26.3	25.1
M4$_{endo}$	7.2	7.3
TS45$_{endo}$	7.4	7.7
M5$_{endo}$	−34.0	−30.9
TS3P$_{endo}$	47.4	45.4
P$_{endo}$	−28.1	−27.1
exo Pathways		
M1	0.0	0.0
TS12$_{exo}$	18.7	15.0
M2$_{exo}$	15.2	12.9
TS23$_{exo}$	21.0	18.3
M3$_{exo}$	6.9	5.7
TS3P$_{exo}$	7.3	6.4
P$_{exo}$	−36.9	−35.4

Table 2. Relative Electronic Energies and Relative Gibbs Energies in Solution (in kcal mol^{-1}) Corresponding to All the Critical Structures Located along the Reaction Coordinate for the THF-Assisted *endo*- and *exo*-Cycloisomerization of 4-Pentyn-1-ol

structures	ΔE_{elec}	ΔG_{soln}
endo Pathways		
M1′	0.0	0.0
TS12′$_{endo}$	19.5	16.9
M2′$_{endo}$	0.0	2.1
TS23′$_{endo}$	3.1	5.6
M3′$_{endo}$	0.1	2.6
TS3P′$_{endo}$	16.3	18.7
P′$_{endo}$	−26.1	−22.1
TS34′$_{endo}$	30.3	28.6
M4′$_{endo}$	11.3	12.0
TS45′$_{endo}$	11.7	12.6
M5′$_{endo}$	−30.4	−28.8
exo Pathways		
M1′	0.0	0.0
TS12′$_{exo}$	14.3	14.0
M2′$_{exo}$	7.9	7.4
TS2P′$_{exo}$	19.8	19.8
P′$_{exo}$	−33.7	−29.7

oxygen atom on the C$_\alpha$ atom. At **M3**$_{endo}$ the O−C$_\alpha$ bond length is 1.704 Å, and the W−C$_\alpha$ bond distance elongates to 2.210 Å, reflecting the weakening of this bond. Finally, **M3**$_{endo}$ evolves into the final product **P**$_{endo}$ through the TS **TS3P**$_{endo}$ (45.4 kcal mol^{-1}) for the hydride transfer from the oxygen to the C$_\beta$. As

a consequence of this H migration, in **P**$_{endo}$ the O−C$_\alpha$ bond distance diminishes to 1.318 Å, while the C$_\alpha$−C$_\beta$ bond length increases from 1.331 to 1.521 Å. The formation of **P**$_{endo}$ from **M1** is exothermic by 27.1 kcal mol^{-1}. The rate-determining step for this process corresponds to **TS3P**$_{endo}$ with an energy barrier of 45.4 kcal mol^{-1}.
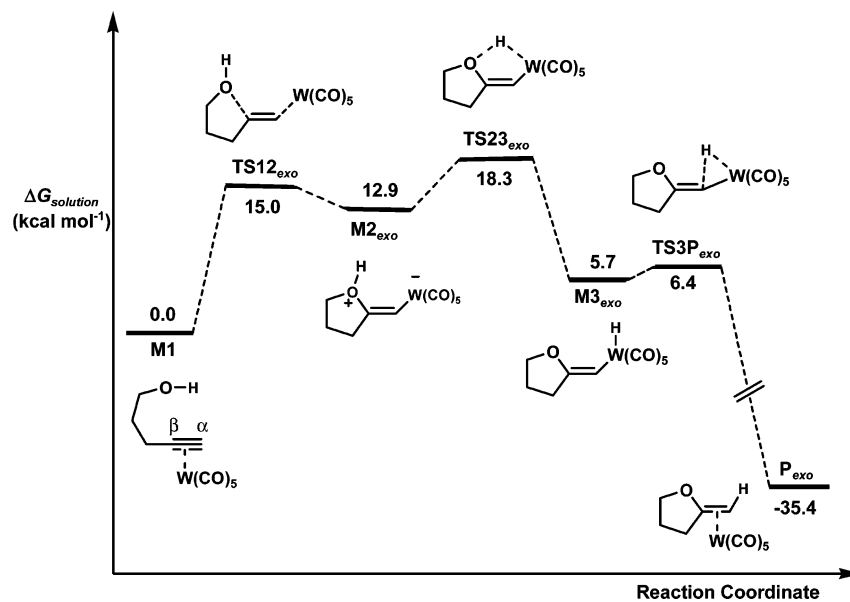
Figure 2. Gibbs energy profile in solution for the *exo*-cycloisomerization of 4-pentyn-1-ol.
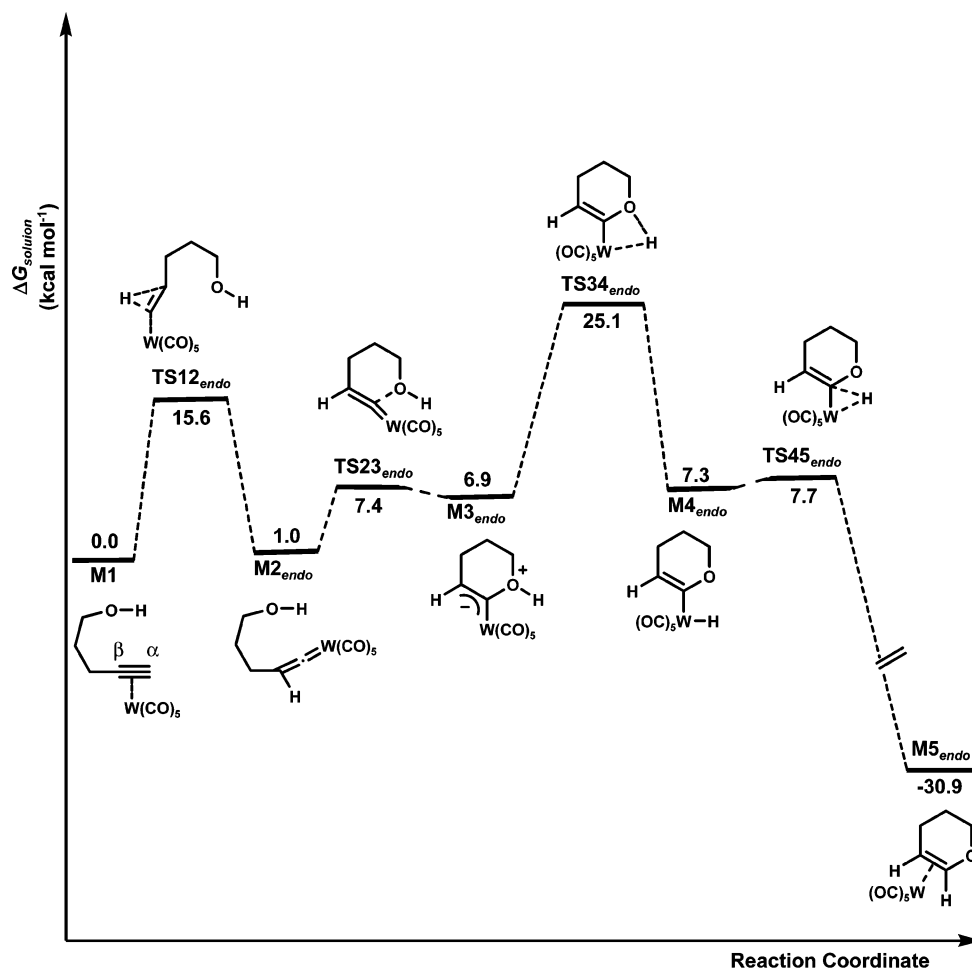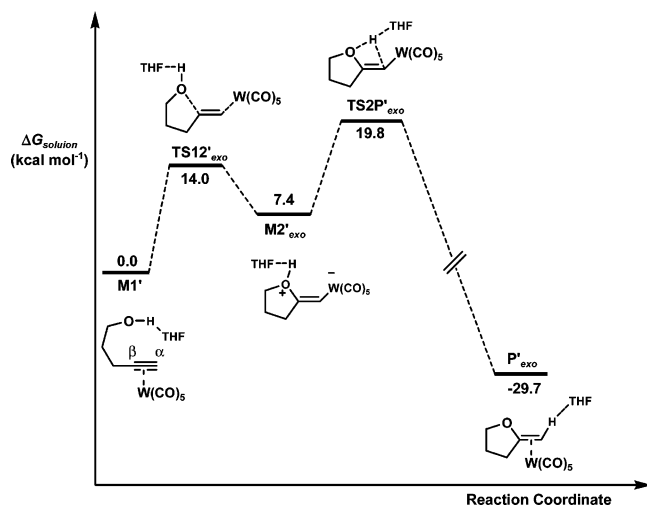

Figure 3. Gibbs energy profile in solution for the *endo*-cycloisomerization of 4-pentyn-1-ol leading to the enol ether **M5**$_{endo}$.

We also found a new *exo* mechanistic route leading from **M1** to the enol ether **P**$_{exo}$ (Figure 2). This route proceeds from **M1** to give the cyclic species **M2**$_{exo}$ (12.9 kcal mol^{-1}) through the TS **TS12**$_{exo}$ (15.0 kcal mol^{-1}) for the intramolecular nucleophilic attack of the oxygen atom on the internal carbon atom of the alkyne moiety. In **M2**$_{exo}$, the C$_\beta$—O distance is 1.538

Å, much shorter than that in **M3**$_{endo}$, and the W atom is coordinated to the C$_\alpha$ atom with a bond distance of 2.286 Å that corresponds to a single bond. A hydride migration from the oxygen to the W center transforms **M2**$_{exo}$ into **M3**$_{exo}$ (5.7 kcal mol^{-1}) through the TS **TS23**$_{exo}$ (18.3 kcal mol^{-1}). As a consequence of this migration, in **M3**$_{exo}$ the C$_\beta$—O distance

Figure 4. Gibbs energy profile in solution for the THF-assisted *exo*-cycloisomerization of 4-pentyn-1-ol.

diminishes to 1.378 Å, and the metal atom presents a pentagonal bipyramidal coordination with two carbonyl ligands in the axial positions. Finally, a reductive elimination through the TS **TS3P$_{exo}$** (6.4 kcal mol^{-1}) gives the *exo* product **P$_{exo}$**. In **P$_{exo}$**, the C$_\beta$–O distance is shorter (1.345 Å) and the C$_\alpha$–C$_\beta$ distance is longer (1.375 Å) than that in **M3$_{exo}$** because of the conjugation of one of the lone pairs of the oxygen atom with the C$_\alpha$–C$_\beta$ π-bond favored by the presence of the metal center. The

formation of **P$_{exo}$** from **M1** is exothermic by 35.4 kcal mol^{-1}. The rate-determining step for this process corresponds to **TS23$_{exo}$** with an energy barrier of 18.3 kcal mol^{-1}.

For comparative purposes we also investigated an *endo* mechanism leading to enol ethers analogous to **2** even though this is not the product experimentally obtained in the absence of an amine. Applying our theory level, we located a mechanistic route (Figure 3) similar in many aspects to that previously reported.[9] This route proceeds from **M1** to the intermediate **M3$_{endo}$** as described above (Figure 1), but now **M3$_{endo}$** (6.9 kcal mol^{-1}) transforms into **M4$_{endo}$** (7.3 kcal mol^{-1}) through the TS **TS34$_{endo}$** (25.1 kcal mol^{-1}) for hydride migration from the oxygen atom to the W center. In **M4$_{endo}$** the C$_\alpha$–O distance diminishes to 1.374 Å, and the metal atom presents a pentagonal bipyramidal coordination with two carbonyl ligands in the axial positions. Finally, a hydride transfer from the W center to the C$_\alpha$ atom gives the final product **M5$_{endo}$** (−30.9 kcal mol^{-1}) through the TS **TS45$_{endo}$** (7.7 kcal mol^{-1}). The rate-determining energy barrier for this process, 25.1 kcal mol^{-1}, corresponds to **TS34$_{endo}$**.

A comparison of the rate-determining energy barriers for the three different mechanisms described above shows that the theoretical model employed yields the *exo* product **P$_{exo}$** as the most favorable one, in sharp contrast with the experimental results.

Given that the rate-determining steps for the three above
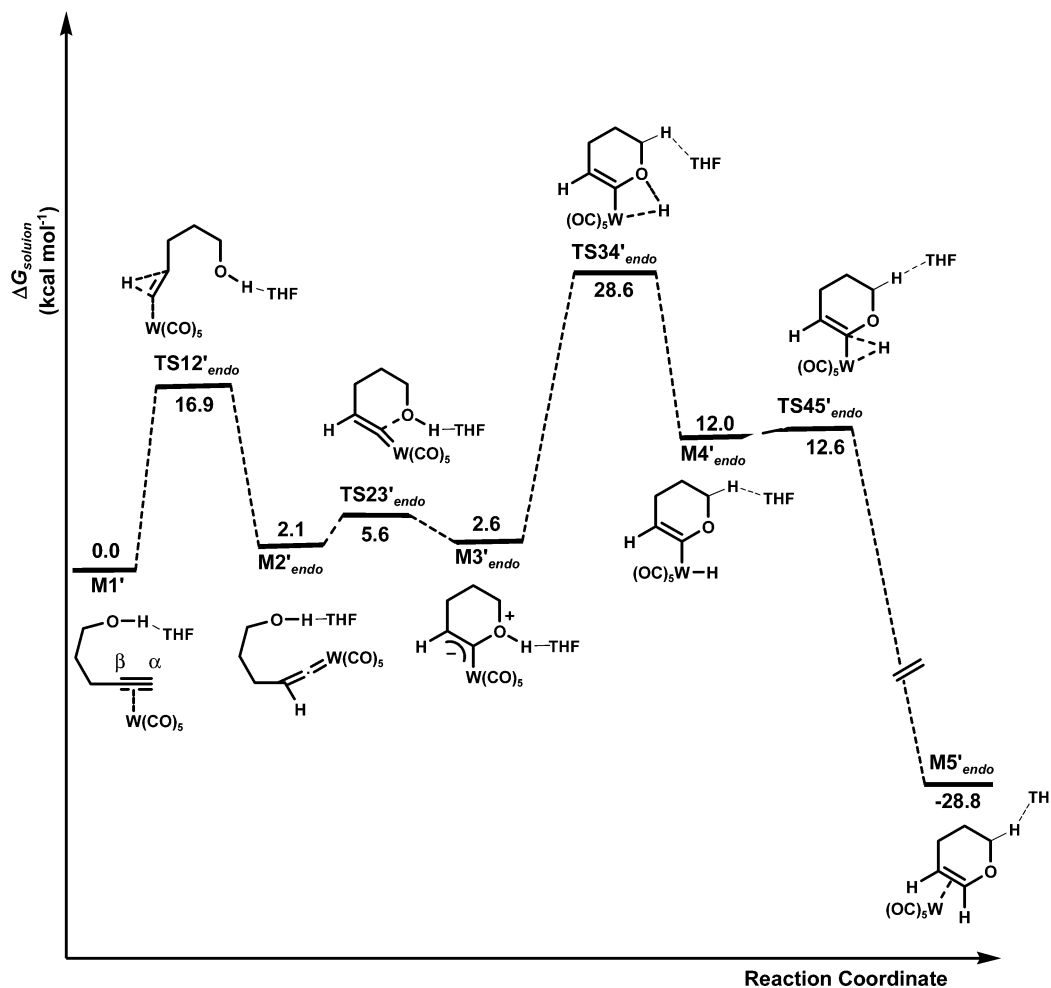
Figure 5. Gibbs energy profile in solution for the THF-assisted *endo*-cycloisomerization of 4-pentyn-1-ol leading to the enol ether **M5$'_{endo}$**.
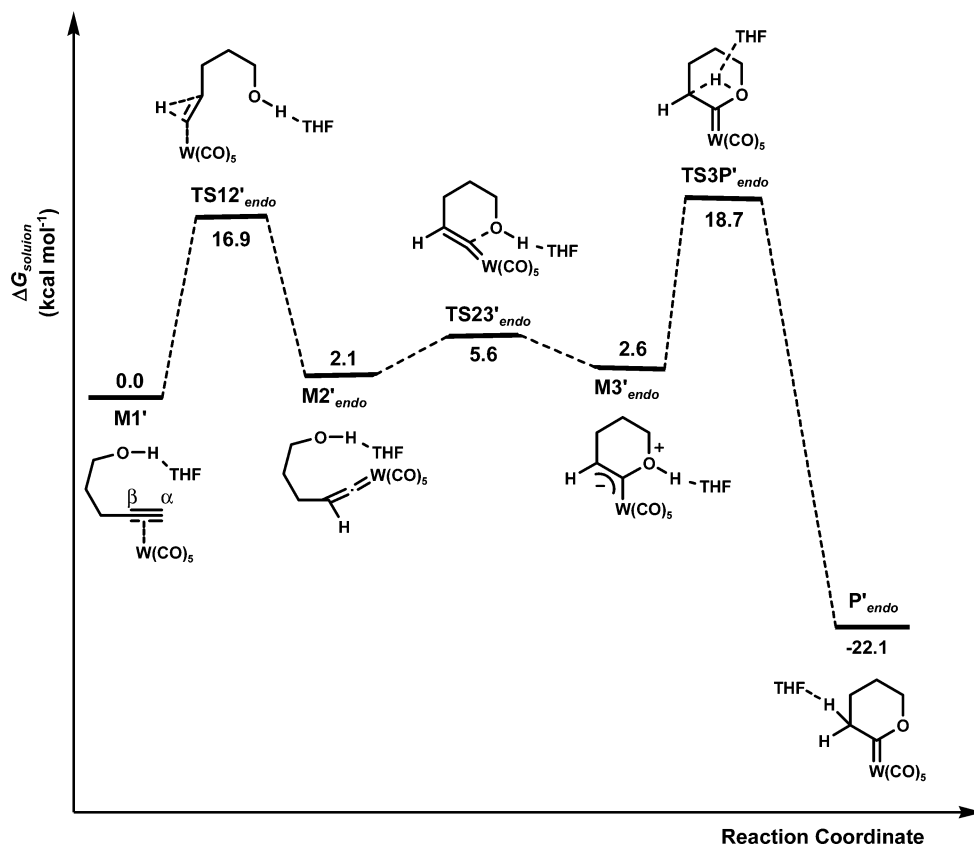
Figure 6. Gibbs energy profile in solution for the THF-assisted *endo-*cycloisomerization of 4-pentyn-1-ol leading to the carbene complex $\mathbf{P}'_{endo}$.

mechanisms correspond to H migrations from oxygen to carbon or tungsten atoms, we thought that solvent molecules could play an active role in the process by assisting those migrations. Therefore, the disagreement between the computational results and experiments obtained above could stem from the inadequacy of the theoretical model employed to reflect that role. Thus, we reinvestigated the *endo-* and *exo-*cycloisomerization of 4-pentyn-1-ol using a mixed model in which a THF molecule was explicitly considered as a component of the reactive system and the effect of bulk solvent was taken into account by the PCM-UAHF method. The critical structures located with this model are displayed in Figures 7 and 8, their names being characterized with a prime symbol.

As before, we initiated our analysis from the alkyne-W(CO)$_5$ complex $\mathbf{M1}'$ with a THF molecule coordinated to the H atom of the hydroxyl group.

As in the *exo* pathway described above, the THF-assisted *exo* mechanism located (Figure 4) proceeds from $\mathbf{M1}'$ to give the cyclic intermediate $\mathbf{M2}'_{exo}$ (7.4 kcal mol^{-1}) through the TS $\mathbf{TS12}'_{exo}$ (14.0 kcal mol^{-1}) so that in this case the assistance of the THF molecule favors the nucleophilic attack of the oxygen atom on the internal carbon atom of the triple bond by 1.0 kcal mol^{-1}. In $\mathbf{M2}'_{exo}$, the interaction of the THF molecule with the hydrogen atom at a distance of 1.511 Å causes the shortening of the C$_\beta$–O bond distance to 1.545 Å. Interestingly, the presence of a THF molecule significantly modifies the mechanism, making more favorable by 3.7 kcal mol^{-1} the direct H transfer from the oxygen to the C$_\alpha$ atom without passing through the metal center so that the system evolves from $\mathbf{M2}'_{exo}$ to $\mathbf{P}'_{exo}$ through $\mathbf{TS2P}'_{exo}$ (19.8 kcal mol^{-1}). At $\mathbf{TS2P}'_{exo}$, the THF molecule interacts with the migrating H atom at a distance of

1.015 Å. The presence of the THF molecule reduces the exothermicity of the process to 29.7 kcal mol^{-1}. The rate-determining TS is now $\mathbf{TS2P}'_{exo}$ with an energy barrier of 19.8 kcal mol^{-1}.
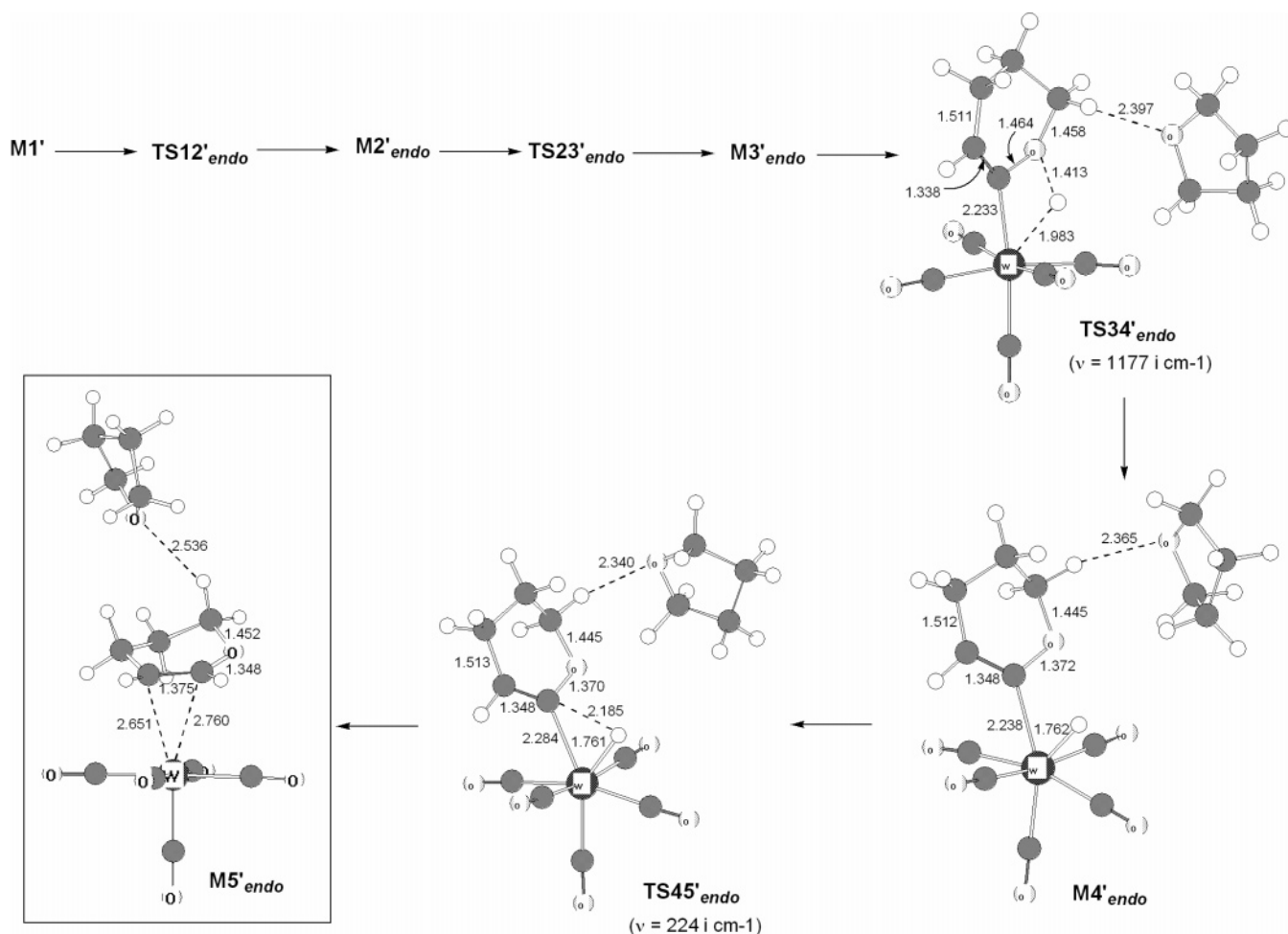
Along the THF-assisted *endo-*cycloisomerization of 4-pentyn-1-ol to yield the enol ether $\mathbf{M5}'_{endo}$ (Figure 5), the system evolves from $\mathbf{M1}'$ through $\mathbf{TS12}'_{endo}$ (16.9 kcal mol^{-1}) to give the vinylidene complex $\mathbf{M2}'_{endo}$ (2.1 kcal mol^{-1}), which in turn transforms into $\mathbf{M3}'_{endo}$ (2.6 kcal mol^{-1}) through $\mathbf{TS23}'_{endo}$ (5.6 kcal mol^{-1}) so that the assistance of the THF molecule favors this intramolecular cyclization by 1.8 kcal mol^{-1}. In $\mathbf{M3}'_{endo}$, the C$_\alpha$–O bond length is reduced to 1.585 Å because of the interaction of the THF molecule with the hydroxylic hydrogen atom at a distance of 1.574 Å. $\mathbf{M3}'_{endo}$ evolves through the TS $\mathbf{TS34}'_{endo}$ (28.6 kcal mol^{-1}) for the H transfer from the oxygen atom to the metal center to yield $\mathbf{M4}'_{endo}$ (12.0 kcal mol^{-1}). It is interesting to note that although the THF molecule was coordinated to the migrating H atom (at a distance of 1.020 Å) at the beginning of the geometry optimization it ends up interacting with one of the H atoms of the methylene group next to the oxygen atom (at a distance of 2.397 Å) where it produces a larger stabilization of the system (Figure 8). Therefore, these results clearly show that in this TS the THF molecule plays no active catalytic role, and consequently, the corresponding energy barrier is even something larger than in its absence (see the energy profile in Figure 3). Finally, $\mathbf{M4}'_{endo}$ yields the enol ether $\mathbf{M5}'_{endo}$ (−28.8 kcal mol^{-1}) through the TS $\mathbf{TS45}'_{endo}$ (12.6 kcal mol^{-1}) for H migration from the metal center to the C$_\alpha$ atom. Thus, the rate-determining energy barrier corresponds to $\mathbf{TS34}'_{endo}$ and amounts to 28.6 kcal mol^{-1}.

The mechanistic route leading from $\mathbf{M1}'$ to $\mathbf{P}'_{endo}$ (Figure 6)
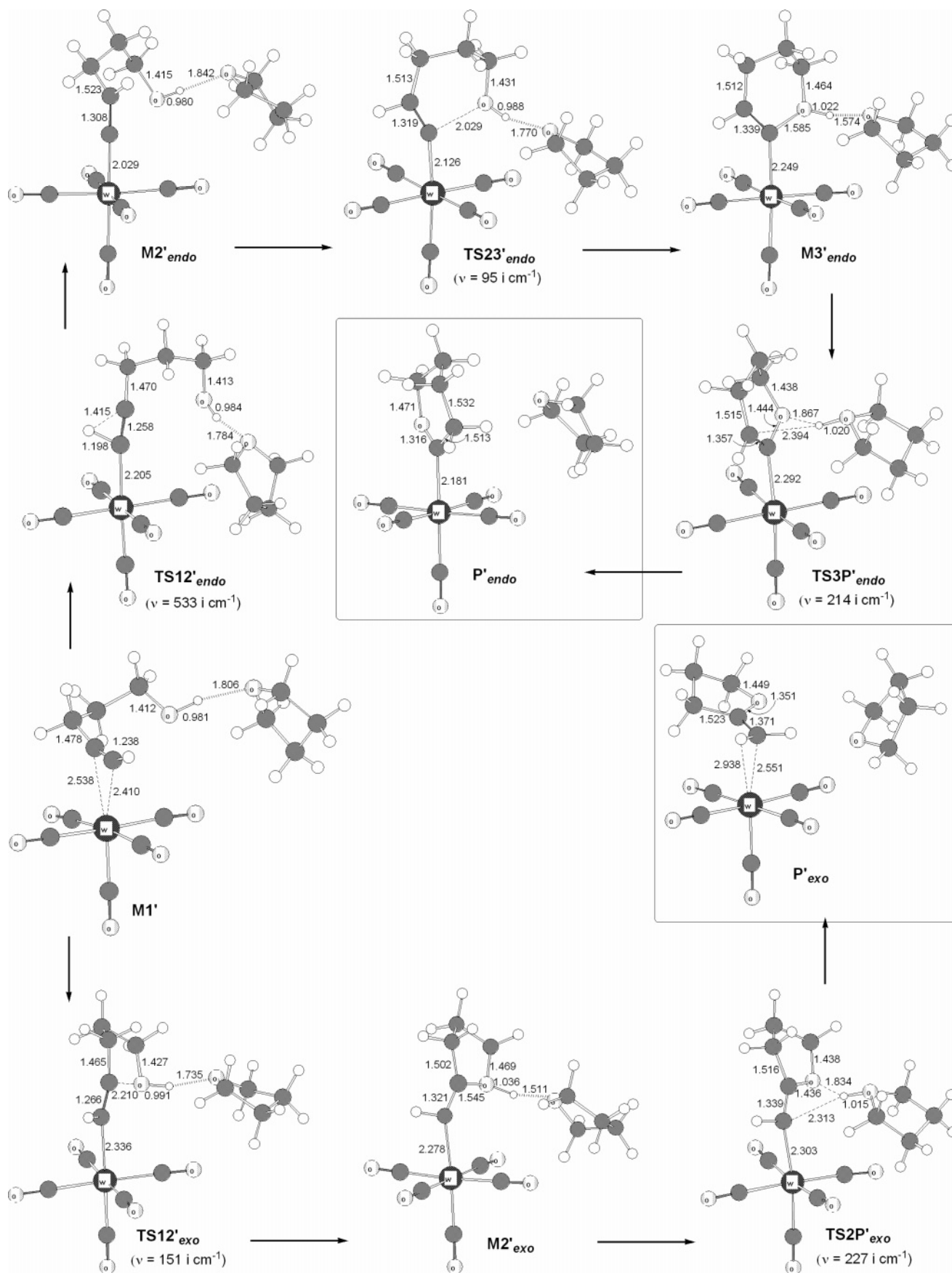
Figure 7. B3LYP optimized geometries of all the critical structures located along the reaction coordinate for the most favorable THF-assisted *endo*- and *exo*-cycloisomerizations of 4-pentyn-1-ol.

Figure 8. B3LYP optimized geometries of all the critical structures located along the reaction coordinate for the THF-assisted *endo*-cycloisomerization of 4-pentyn-1-ol leading to $\mathbf{M5'_{endo}}$.

proceeds through $\mathbf{TS12'_{endo}} \rightarrow \mathbf{M2'_{endo}} \rightarrow \mathbf{TS23'_{endo}} \rightarrow \mathbf{M3'_{endo}}$ as above, but now the hydroxylic hydrogen atom migrates directly to the C_β atom through $\mathbf{TS3P'_{endo}}$ (18.7 kcal mol^{-1}) to yield the final product $\mathbf{P'_{endo}}$. Therefore, the assistance of the THF molecule produces a reduction of 26.7 kcal mol^{-1} in the energy barrier of $\mathbf{TS3P'_{endo}}$. At $\mathbf{TS3P'_{endo}}$, the THF molecule interacts with the migrating H atom at a distance of 1.020 Å. The presence of the THF molecule reduces the exothermicity of the formation of this carbene complex to 22.1 kcal mol^{-1}. The rate-determining energy barrier corresponds to $\mathbf{TS3P'_{endo}}$ and amounts to 18.7 kcal mol^{-1}.

Thus, from the above results we see that thanks to a crucial catalytic action, the THF molecule favors the direct hydride migration to the C_β atom through $\mathbf{TS3P'_{endo}}$ to yield the carbene complex $\mathbf{P'_{endo}}$ over the hydride migration through the metal center to yield the enol ether $\mathbf{M5'_{endo}}$.

Therefore, the computational results rendered by this mixed model are able to rationalize the experimental findings. On one hand, the cyclic carbene complex $\mathbf{P'_{endo}}$ is the most favored one, and on the other hand, the difference in the rate-limiting energy barriers for the most favorable *endo* and *exo* routes (1.1 kcal mol^{-1}) could explain the fact that mixtures of both products are obtained depending on the substituents on the carbon backbone, the experimental conditions, etc.

Conclusions

In the present work, we report new mechanistic routes for the (THF)W(CO)$_5$-promoted *endo-* and *exo-*cycloisomerization of 4-pentyn-1-ol assisted by a THF molecule. To investigate the specific role played by THF molecules in this reaction, we have employed a mixed model in which one THF molecule is initially coordinated to the hydroxyl hydrogen atom while bulk solvent effects are evaluated by the PCM-UAHF method.

The assistance of the THF molecule in the formation of the *exo* product facilitates the intramolecular nucleophilic attack of the oxygen atom in the first step of the process by 1.0 kcal mol^{-1} and modifies the mechanism for the H transfer from the oxygen atom to the carbon atom bonded to W, making more favorable the direct transfer without passing through the metal atom. Along the *endo*-cycloisomerization the THF molecule assistance makes easier again the intramolecular nucleophilic attack of oxygen by 1.8 kcal mol^{-1} and, thanks to a crucial catalytic action that reduces by 26.7 kcal mol^{-1} the energy barrier for the direct hydride migration to the C_β atom, favors the route to the carbene complex over the formation of the enol ether.

These new mechanisms make possible the satisfactory rationalization of experimental results giving the *endo* pathway as the most favorable one and rendering a difference between

the rate-determining barriers for the *endo* and *exo* routes (1.1 kcal mol^{-1}), which allows us to explain the fact that different mixtures of *endo* and *exo* products are obtained depending on the substituents on the carbon backbone, the experimental conditions, etc.

Supporting Information Available: Optimized structures, absolute electronic energies, ZPVE corrections, and relative Gibbs energies in the gas phase of all the critical structures located in this work. This material is available free of charge via the Internet at http://pubs.acs.org.

JA045567K